

## Human Factor VIII: Morphometric Analysis of Purified Material in Solution

**Abstract.** Study of purified human factor VIII in buffer by freeze-etch electron microscopy reveals rounded, rod-shaped particles measuring 22 by 42 nanometers. When thrombin was added to purified normal factor VIII, there was a rapid loss of rod-shaped particles during the first 15 minutes of incubation at 37°C. Purified plasma from two patients with severe hemophilia contained spherical particles measuring 10 to 50 nanometers in diameter, with no evidence of significant numbers of rod-shaped forms. Negatively stained and unstained air-dried samples of factor VIII corroborate the relative shape and size differences between normal and hemophilic material.

Factor VIII is necessary for normal blood coagulation as well as platelet function. Reduced levels of procoagulant factor VIII (FVIII) are associated with two disease states in man, hemophilia and von Willebrand's disease. In addition to its procoagulant function, FVIII has von Willebrand factor activity (vWf) as well as single or multiple immunologic sites of reaction to heterologous antibodies to FVIII (1-3). Von Willebrand factor activity may be characterized by defective aggregation of platelet-rich plasma in response to the antibiotic ristocetin in patients with von Willebrand's disease as compared to normal. The older term antihemophilic factor now comprises both procoagulant as well as von Willebrand factor activities (FVIII/vWf). Human FVIII/vWf has been characterized as a macromolecule whose molecular weight is at least 1.2 million. When reduced with dithioerythritol or 2-mercaptoethanol, a single subunit with a molecular weight of approximately 230,000 appears upon electrophoresis in 3 percent polyacrylamide gels (1-3). It is uncertain, at present, whether procoagulant and von Willebrand factor activities reside on the same or separate, but related, molecules (1-4). Further analysis of FVIII/vWf has been hindered by the paucity of objective, nonphenomenological assays of purity in the material examined. As an initial attempt at resolving this difficulty, we examined the morphometric features of highly purified normal human FVIII/vWf in buffer solution by the freeze-etch technique (5). It should be emphasized that data obtained by this method represent information on unfixed material in solution. There is no drying, staining, or fixation artifact. The amenability of FVIII/vWf to this method of analysis is fortuitous and probably is the result of the presumed large size and high molecular weight of the molecule as well as other undetermined factors. In order to corroborate the information from freeze-etch specimens, all material was submitted to

negative staining, and unstained bright- and darkfield low-exposure electron microscopy of air-dried droplets of FVIII/vWf in buffer on carbon-coated grids.

Pooled, human FVIII/vWf was purified by the method of Shapiro *et al.* (2). FVIII/vWf showing more than 10,000-fold increase in specific activity was obtained in a tris-NaCl buffer at pH 7.4 (0.05M tris, 0.5M NaCl, 0.1M  $\epsilon$ -aminocaproic acid and 0.2 percent NaN<sub>3</sub>). Purified material reduced with 2-mercaptoethanol and applied to 3 percent polyacrylamide gels in the presence of sodium dodecyl sulfate showed a single band whose approximate molecular weight was 230,000. After adjustment to a final protein concentration of 150 to 175 mg per 100 ml, 5- $\mu$ l portions of the FVIII/vWf buffer mixture were frozen in specimen holders in Freon 22 at -190°C. Freeze-etch carbon platinum replicas of FVIII/vWf in buffer mixture showed many rod-shaped rounded particles. Most particles were bent at variable intervals along their length at approximately 90° and 120° angles. Ends of particles were usually rounded with a somewhat greater diameter than the rest of the structure (Fig. 1). Examination of images of FVIII/vWf in solution represents morphological analysis in three dimensions. Figure 1 shows particles in all positions from horizontal to perpendicular. Measurement of particle width shows an average upper limit of 22 nm. Smaller widths were always associated with smaller spherical particles. These could represent a second family of non-rod-shaped particles or the tips of rod-shaped particles just being revealed by the receding, sublimating, buffer solution. Examination of particles with rod shapes reveals that approximately 70 percent of the total were 42 nm long. Of the remainder, 20 percent measure approximately 55 nm in length and 10 percent measure 67 nm. All rod-shaped structures were about 22 nm in width. Since there is a 3-nm layer of carbon platinum on the actual particles in the buffer, the coefficient

of error in the measurements given is equal to this value. Measurement of thickness was made by the quartz crystal thin-film monitor QSG 201 (Balzers) (6).

Examination of FVIII/vWf by negative staining with phosphotungstic acid (PTA) at pH 2.3 and pH 7.0 showed oval and rounded rod-shaped structures approximately one and one-half times the size of freeze-etch particles. Outlines were smooth but did not show the 90° and 120° angles found in freeze-etch structures. Unstained air-dried FVIII/vWf examined by brightfield and darkfield electron microscopy (7) revealed structures surprisingly similar to freeze-etch images. The outlines of these air-dried particles were straighter, however, while the ends were larger and generally less rounded. Bends of approximately 90° or 120° appeared in most structures (Fig. 2). Outlines of unstained and stained material were generally similar except for the absence of angulation in the latter. We are uncertain of what caused this. It is possible that air drying plus interaction of buffer and FVIII during drying results in the collapse of a three-dimensional structure into an essentially two-dimensional one. The lack of angulation in stained specimens might result from the support given to the particles by the stain. Analysis of unstained images also showed a complex but regular pattern of parallel electron-opaque lines spaced at 2.5-nm intervals that intersect with similar lines at right angles (Fig. 2). These form what can be called a cross-hatch lattice pattern. These patterns were not seen by negative staining. Less frequently, parallel electron-opaque lines were observed within rod-shaped particles and these did not intersect at right angles with other lines (Fig. 2). Because unstained low-exposure electron microscopy is associated with continuous and culminative radiation damage to examined material, care must be exercised in interpretation. Although precautions were taken to minimize this effect (8), both crosshatch and parallel electron-opaque linear lines probably result, in part, from a continuous thermal effect produced by the incident electron beam. In general, negative stain images appear less distinct and fewer in number than unstained images. Demonstration of negative stain images depends on density differences between stain and object. The peculiar clarity of unstained images and the lack of distinction of negative stain images indicates that air-dried material may approximate the electron density of PTA stain.

Although we can identify FVIII/vWf

with these rod-shaped particles on the basis of high concentration and relative uniformity of the observed structures in the buffer solution, additional proof is necessary. Controls prepared with freeze-etch and air-dried specimens of distilled water, tris buffer with and without  $\text{NaN}_3$ , albumin, normal human plasma, fibrinogen, and gamma globulin failed to reveal the particles described above. Similarly, centrifugation to remove possible platelet fragment contaminants during the purification procedure were performed. Extraction with chloroform at appropriate steps during purification failed to alter the character of the particles. Since thrombin changes the activity of FVIII/vWf over time, we repeated the experiment of Andersen and McKee (8) with the same techniques. Portions ( $5 \mu\text{l}$ ) of FVIII/vWf in tris-NaCl buffer at  $37^\circ\text{C}$  were removed at the start, at 15 seconds, at 2, 5, 10, 15, 30, and 60 minutes, and at 24 hours before and after the addition of 0.1 NIH units of thrombin per milliliter. Results show a rapid loss of rod-shaped particles during the first 15 minutes of incubation. After 15 minutes incubation mixtures showed decreasing numbers of predominantly spherical particles measuring 10 to 20 nm in diameter. Corresponding determination of procoagulant activity showed a decrease to less than half of initial values at 15 minutes of incubation. Biological activity in the 24-hour specimen was absent. Control incubation of FVIII/vWf without thrombin at  $37^\circ\text{C}$  for corresponding intervals up to 24 hours showed some loss of rod-shaped particles without the marked decrease noted in thrombin-treated material. Biologic activity in these specimens was decreased to one-quarter of initial values. The 24-hour specimen also showed a decrease in the number of observable particles. Simple freezing and thawing of FVIII/vWf before freezing in Freon 22 and liquid nitrogen also resulted in a decrease in the number of rod-shaped particles to a lower concentration when the FVIII/vWf buffer mixture showed a protein concentration of 90 mg per 100 ml. All studies, with the exception of the analysis of FVIII/vWf from the single normal donor, were performed twice.

Examination of purified plasma obtained from two patients with severe hemophilia failed to show significant numbers of rod-shaped structures. Instead, spherical particles 10 to 50 nm in diameter were evident (Fig. 3). Larger forms frequently appeared to have flattened sides. Occasionally, after extensive search, a rod-shaped particle was identi-

fied. A control freeze-fracture experiment on material purified from a mixture of half normal and half hemophiliac plasma revealed a mixture of small to large, spherical or rhomboid forms and rod-shaped particles. Unstained low-exposure electron microscopy failed to reveal the crosshatch lattice pattern of normal FVIII/vWf (Fig. 4). Occasional single electron-opaque lines were present in occasional spherical particles from hemophiliac material. We hypothesize that these dissimilarities between normal and hemophiliac FVIII/vWf material may be caused by differences in subunit organization or biochemical composition.

Normal FVIII/vWf, after purification, is thought to have a molecular weight of at least 1.2 million (1-3, 9). After reduction, a single band forms in sodium dodecyl sulfate polyacrylamide gels, indicating a common subunit structure whose molecular weight is approximately 230,000 (1-3, 9). In normal individuals, rod-shaped particles measuring 22 by 42 nm showed a molecular weight of approximately 8.5 million (upper limit) when suspended in buffer mixture. By contrast, purified plasma obtained from the two patients with severe hemophilia shows particles whose molecular weight (upper limit) is approximately 1 to 20 million. It should be pointed out that the

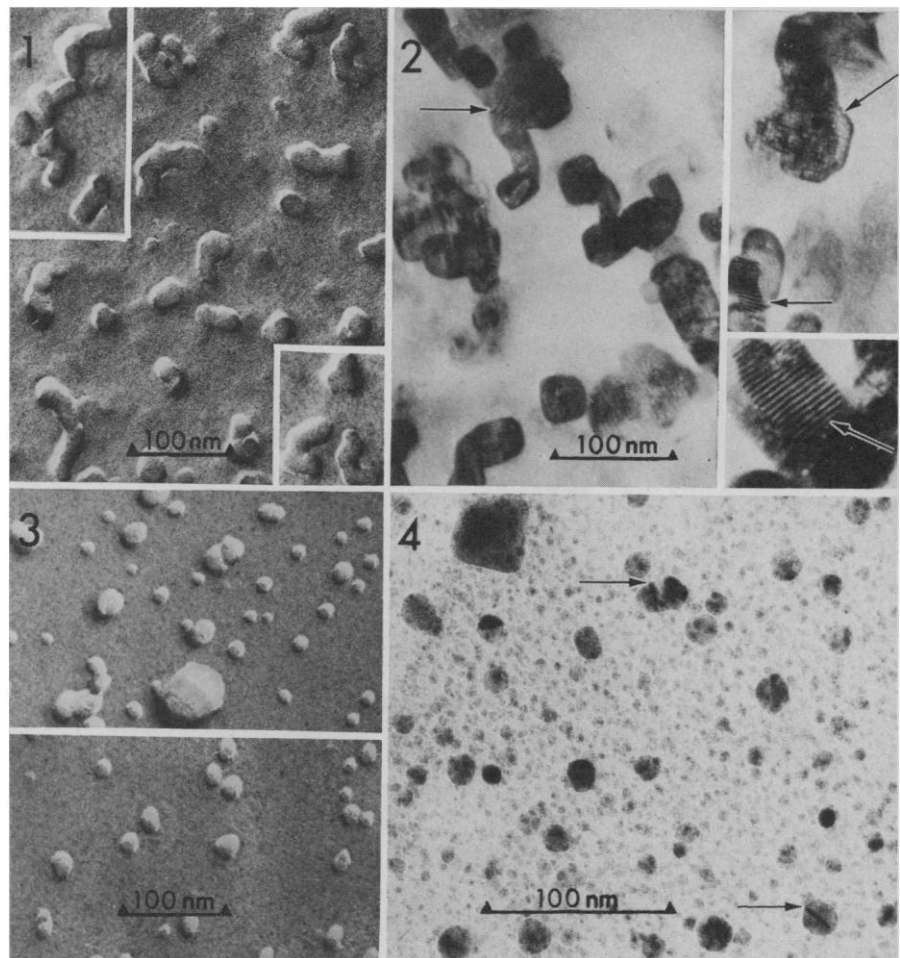


Fig. 1. Freeze-etch replica of normal purified human factor VIII (FVIII/vWf) in buffer. Rod-shaped particles with and without bends at approximately  $90^\circ$  and  $120^\circ$  angles are present. Spherical particles of smaller diameter are present throughout plane of replica. The insets demonstrate additional configurations of rod-shaped particles. Fig. 2. Unstained low-exposure electron microscopy of normal purified FVIII/vWf. The larger picture shows greater size but similar shape and angulation of bends of particles when compared to Fig. 1. The parallel dark lines within particles are indicated by arrow. The upper right inset demonstrates cross-hatch lattice pattern (upper arrow). An occasional particle shows heavy electron-opaque parallel internal lines (lower arrow). The lower right inset, at higher magnification, shows details of parallel electron-opaque lines within the particle. Fig. 3. Freeze-etch replica of purified plasma from patient with severe hemophilia. The upper and lower photographs show predominantly spherical shapes of variable size. Fig. 4. Unstained low-exposure electron microscopy of purified plasma from patient with severe hemophilia. There is an absence of structures similar to those in Fig. 2. Many spherical shapes are evident. Occasional images demonstrate single or double parallel electron-opaque lines internally (arrows).

molecular weights of FVIII/vWf and hemophilic material may be much less than the upper limit given. Moreover, there may not be any simple relation between the molecular weights of FVIII/vWf and hemophilic material of similar dimensions. Hence, these results do not necessarily conflict with the observation that both hemophilic FVIII and normal FVIII have molecular weights of at least 1.2 million and behave similarly on gel filtration (9). Thus, the primary distinction appears to be one of a different quaternary structure for normal compared to hemophilic material. Some corroboration of this might be indicated by the difference between internal images of normal and hemophilic material on low-exposure microscopy. Whether this difference, derived from concentrated purified FVIII/vWf in buffer, is present in vivo cannot be ascertained. It is not possible, at present, to derive further information from the available data without overinterpretation of essentially morphological differences. We caution that far greater numbers of normal and abnormal plasmas, purified by different techniques, must be examined before significant differences may be claimed. We suggest that the combination of techniques used in our study should be useful in the analysis of normal and disease states associated with the FVIII/vWf molecule.

HENRY K. TAN\*

JUDITH C. ANDERSEN†

Hematology Section, Clinical Pathology Department, National Institutes of Health, Bethesda, Maryland 20014

#### References and Notes

- O. D. Ratnoff, L. Kass, P. D. Lang, *J. Clin. Invest.* **48**, 957 (1969); M. E. Legaz, R. B. Schmer, R. B. Counts, E. W. Davie, *J. Biol. Chem.* **248**, 3946 (1973).
  - G. A. Shapiro, J. C. Andersen, S. V. Pizzo, P. A. McKee, *J. Clin. Invest.* **52**, 2198 (1973).
  - S. L. Marchesi, N. R. Shulman, H. R. Grainick, *ibid.* **51**, 2151 (1972).
  - M. E. Switzer and P. A. McKee, *ibid.* **57**, 925 (1976).
  - E. L. Benedetti and P. Favard, *Freeze-Etching, Techniques and Applications* (Societe Francaise de Microscopie Electronique, Paris, 1973).
  - Quartz crystal thin-film monitor QSG 201 (Balzers, Liechtenstein) was used in conjunction with electron beam evaporation equipment EVM 052 (Balzers) and electron beam gun EK 552 (Balzers) for precise control and monitoring of carbon platinum film layer. All freeze-etch procedures were carried out in a Balzers BAF 300 high-vacuum freeze-etch unit equipped with a turbomolecular pump and examined with a Zeiss EM 10 electron microscope (Carl Zeiss, Oberkochen, West Germany).
  - R. C. Williams and H. W. Fisher, *J. Mol. Biol.* **52**, 121 (1970).
  - J. C. Andersen and P. A. McKee, *Circulation* **46** (Suppl. 2), 52 (1972).
  - L. Kass, O. D. Ratnoff, M. A. Leon, *J. Clin. Invest.* **48**, 351 (1969).
- \* Present address: Laboratory of Molecular Immunology, Scripps Clinic and Research Foundation, La Jolla, Calif. 92037.  
 † Present address: Hematology Section, Department of Medicine, Duke University School of Medicine, Durham, N.C.

19 April 1977; revised 1 July 1977

## Cigarette Smoke Activates Guanylate Cyclase and Increases Guanosine 3',5'-Monophosphate in Tissues

**Abstract.** *The gaseous phase of cigarette smoke induced a 2- to 36-fold increase in the activity of guanylate cyclase in supernatant and particulate fractions from various rat and bovine tissues over basal activity. The characteristics of this phenomenon paralleled those of the activation of guanylate cyclase by nitric oxide, which is a component of tobacco smoke.*

Guanylate cyclase (E.C. 4.6.1.2), the enzyme that catalyses the formation of guanosine 3',5'-monophosphate (cyclic GMP) from guanosine triphosphate and its product are incompletely understood. Although the concentrations of guanylate cyclase and cyclic GMP are increased in tumors and proliferating tissues (1) and in tissues exposed to certain smooth muscle relaxing agents, including sodium nitroprusside and nitroglycerin (2), the physiological implications of these observations are unclear. Compounds capable of forming nitroso compounds, compounds containing nitroso groups (some of which are carcinogenic), and nitric oxide (NO) gas are all able to increase guanylate cyclase activity and cyclic GMP levels (2-4). The common mechanism for this activation is thought to be the formation of NO (4).

The gas phase of fresh cigarette smoke contains NO but minimal amounts, if any, of the higher oxides of nitrogen (5). We report here that the gas phase of cigarette smoke causes a 2- to 36-fold in-

crease in the activity of guanylate cyclase in preparations of broken cells from various rat and bovine tissues, and increases cyclic GMP but not adenosine 3',5'-monophosphate (cyclic AMP) in minced rat lung. The characteristics of this activation are similar, both qualitatively and quantitatively to those reported for NO (4) with respect to the extent of activation, tissue specificity, and activity in the presence of various compounds that alter the activation of guanylate cyclase by NO. Other workers have demonstrated the induction of aryl hydrocarbon hydroxylase in lung preparations by particulate components of cigarette smoke (6). However, our experiments suggest that NO is the component of cigarette smoke vapor that activates the guanylate cyclase.

Male Sprague-Dawley rats were decapitated, and the tissues, except as indicated in Table 1, were processed as described (4) to obtain supernatant and particulate fractions (separated at 105,000g). Bovine pulmonary structures were obtained at a local abattoir and were processed in the same way. Guanylate cyclase and adenylate cyclase (E.C. 4.6.1.1) activities were determined as described (4) in 100- $\mu$ l reaction mixtures containing enzyme, 1 mM guanosine triphosphate or adenosine triphosphate, 4 mM MnCl<sub>2</sub>, 50 mM tris-HCl buffer (pH 7.6), 10 mM theophylline, 15 mM creatine phosphate, 20  $\mu$ g of creatine phosphokinase (E.C. 2.7.3.2; 120 to 130 unit/mg) and other compounds at the concentrations indicated. Nitric oxide gas (Matheson Gas Products) was introduced 1 cm above some reaction mixtures as reported previously (4). Various brands of filter cigarettes were held in a plastic pipette tip containing a loosely packed, 40-mg glass wool plug. Smoke was drawn from the cigarette through the glass wool plug and Millipore AP 200 2500 glass fiber discs in order to eliminate the particulate fraction of smoke. The fresh gas phase of the smoke was introduced 1 cm above the reaction mixture contained in closed tubes (10 by 75 mm). The atmosphere in the tubes was 98 to 99 percent smoke vapor and 1 to 2 percent room air. The design of the system for the delivery of smoke is similar

Table 1. Effect of cigarette smoke vapor and nitric oxide gas on cyclic GMP and cyclic AMP concentrations in rat lung. Fresh rat lung was placed in cold Krebs-Ringer solution containing glucose (2 mg/ml) and 50 mM tris-HCl, pH 7.6. Minced tissue (0.3 by 0.3 mm) was prepared with a McIlwain chopper and placed in fresh Krebs-Ringer solution for 15 minutes. The minced tissue containing 2 to 5 mg of protein was then transferred to tubes (15 by 85 mm) containing 1 ml of fresh medium and incubated for 3 minutes. Some tubes were exposed to 100 percent N<sub>2</sub> for 10 seconds, some to 100 percent N<sub>2</sub>, 417  $\mu$ l of NO, and 100 percent N<sub>2</sub> for 10 seconds each, and some to 98 percent cigarette smoke vapor from brand D for 30 seconds. All tubes were capped for the first 30 seconds to confine the desired atmosphere. Reactions were terminated with 0.5 ml of 18 percent trichloroacetic acid. The supernatant fractions were extracted and assayed for cyclic nucleotides (4, 9). All experiments were done in triplicate, and the values are the means  $\pm$  standard error of three determinations.

Addition	Cyclic nucleotides (pmole/mg protein)	
	GMP	AMP
None	0.08 $\pm$ 0.01	2.30 $\pm$ 0.35
NO	6.38 $\pm$ 0.73*	2.01 $\pm$ 0.01
Smoke	1.06 $\pm$ 0.17*	2.21 $\pm$ 0.02

\*P < .02.